Journal of Materials Chemistry A

ROYAL SOCIETY OF CHEMISTRY

PAPER

View Article Online
View Journal | View Issue

Cite this: J. Mater. Chem. A, 2023, 11, 5725

Ion transport and growth behavior of solid electrolyte interphases on Li and Na with liquid electrolytes based on impedance analysis†‡

Kyungmi Lim, Jelena Popovic §* and Joachim Maier

Electrochemical impedance spectroscopy (EIS) is an irreplaceable tool for investigating ion transport mechanism and growth of solid electrolyte interphases (SEIs) on Li or Na electrodes. Nevertheless, studies providing understanding of the EIS response and establishing a proper equivalent circuit models for SEIs are rare. In this study, using already published and new data, we develop a most simplified, but suitable EIS model by focusing not only on the measured resistances but also on the corresponding activation energies of ion transport and the respective capacitances. The equivalent circuit model takes account of channels filled with liquid electrolyte in parallel with the more resistive bulk parts of the SEI. The growth of initially porous SEIs proceeds at the liquid/solid interface in the channel, where an additional thin passivation layer (for example native film) may exist. The channels (in reality pores of solid SEI) are either eventually filled, or, if the products from the reaction between liquid electrolytes and alkali metals possess a very different molar volume compared to the already-existing material (Li or Na), another internally porous SEI structure forms. The first scenario seems rather typical for Li, in particular at longer growth times. The latter potentially self-similar-growth behavior seems to apply for contacts of glyme-based liquid electrolyte with Na. Inclusion of the lateral compaction effects in an extended model allows for remarkably good description for the Na/glyme scenario.

Received 25th November 2022
Accepted 13th February 2023

DOI: 10.1039/d2ta09189e

rsc.li/materials-a

1. Introduction

Battery technology continuously changes our lives by enabling the easier use of portable electronic devices and electric vehicles, as well as enabling fossil fuel-free economy.[1,2] Despite the substantial improvement of energy density of batteries over the years, the fundamental understanding of the exact physical origin of the overpotential in the battery cells is still insufficient.[3–5] The overpotential is determined by a variety of kinetic factors including ohmic drop, charge transfer at interfaces, charge transport within the crystal structure of materials (solid-state diffusion), concentration polarization in electrolytes and additional parasitic reactions.[4,6,7] Electrochemical impedance spectroscopy (EIS) is a powerful technique for achieving a more detailed understanding of the electrical transport, since it allows decoupling of kinetic processes with different relaxation times by measurement at a wide frequency range (MHz to mHz).[8–11] In particular, EIS is an indispensable method for the investigation of the solid electrolyte interphase (SEI), the organic/inorganic thin passivation layer formed by the (electro) chemical decomposition of electrolyte in contact with the respective electrode.[12–14] The experimental difficulties of SEI studies include air-sensitivity and the inherently complex and fragile SEI morphology composed of many chemical compounds with variable mechanical properties and sometimes non-negligible amount of pores.[15–23] The above mentioned problems pose even greater challenges for the studies of SEIs on the reactive Li/Na metals, currently considered to be the attractive anode materials for future-generation batteries.[24–28] Although novel experimental strategies such as cryo-transmission electron microscopy (TEM),[29–32] X-ray-based analytical tools[33–35] and nuclear magnetic resonance (NMR) spectroscopy have been recently applied in SEI research,[32,36–40] EIS offers particular advantages, as it enables us to distinguish between different electrochemical transport processes *in situ* and in a non-destructive way.[10,41–43]

Recently, we collected evidence that SEIs on the alkali metals are porous, especially for the Na case.[44] The corresponding equivalent circuit model based on the so far not published data, as well as their growth mechanisms will be discussed in this paper. Very general models, such as a transmission line model, have frequently been used to treat the ionic transport in porous electrodes. However, given the high complexity of the system, the parametrization of such models remains difficult.[45–50]

Max Planck Institute for Solid State Research, 70569 Stuttgart, Germany. E-mail: popovic@fkf.mpg.de; jelena.popovic-neuber@uis.no

† Dedicated to Prof. Doron Aurbach for his 70th birthday.

‡ Electronic supplementary information (ESI) available. See DOI: https://doi.org/10.1039/d2ta09189e

§ Current address: University of Stavanger, Department of Energy and Petroleum Engineering, Stavanger, Norway.

Rather than applying such a deductive approach, we follow an inductive approach, which is based on a most simplified equivalent circuit which contains a minimum number of circuit elements. Guided by the values of activation energy and relaxation times, which enable us to identify the major transport pathways, we chose the basic motif to be as simple as possible, and make it more complex only if it appears unavoidable. In addition to studying initial structures, we follow and discuss the growth behavior of SEIs on Li/Na over time under open circuit potential (OCP) from the EIS data and give suggestions about the feasible morphological changes of the SEI. Using such simple concepts, the growth behavior of the systems under concern can be described amazingly well on a semi-quantitative level. We highlight the importance of measuring the activation energy (E_a) and inspecting the capacitances, since these parameters provide insight into the dominant ionic transport pathways and the morphology of the SEIs.

2. Results and discussion

2.1. Equivalent circuit model for ion transport in the SEI

Li and Na electrodes were contacted with two types of liquid electrolytes (glyme-based and carbonate-based) and the resulting symmetric cells were measured with EIS. The experimental details were given in a previous publication and can also be found in the ESI.‡[44] The initial impedance spectra are shown in the ESI (Fig. S1‡), where only a single semicircle is observed in the Nyquist plot for the measured frequency range (10^6∼1 Hz). The semicircle corresponds to transport in the SEI as supported by the values of capacitances which are in the range of 10^{-7} to 10^{-6} F cm^{-2},[51] and the values of relaxation times (Fig. 2, will be discussed later), which do not correspond to the ion transport in bulk liquid electrolyte or to the concentration polarization (*e.g.* in bulk liquid electrolyte or in liquid electrolyte inside of open-pores, see Fig. S1‡ for more details). However, for the situation when some or many pores are closed (*e.g.* liquid electrolyte encapsulated in solid SEI), such concentration polarization may not be negligible. We also neglect current constriction phenomena, as we expect a large number of closely packed pores. In our previous study, we proved that SEIs on Na metal electrodes formed by the contact with glyme- and carbonate-based salt-in-solvent electrolytes are porous directly after assembly, and remain porous even after the symmetric electrochemical cell was aged under OCP for 600 hours.[44] This finding was supported by the measured activation energy of ionic transport in the SEI (E_a(SEI)) (0.15–0.3 eV for the initial storage with Na, showing values close to the ones of the respective liquid electrolyte). Further corroboration stems from focused-ion beam-scanning electron microscopy (FIB-SEM) images, where a number of larger pores (*ca.* 50 nm) were visible.[44] Thus, the SEI semicircle observed for SEI on Na metal should not be interpreted as just a contribution of composite material of several solid phases, as previously suggested for Li metal.[52–54] Such SEI semicircle rather corresponds to a complex transport through a solid–liquid composite material.

In order to model our EIS data, we start out with the most meaningful parameter as far as the identification of the rate determining step of ion transport through the SEI is concerned, namely the E_a, derived from the temperature dependence of the (temperature)/(diameter of the semicircle arc) from our previous publication. The most striking difference between the Li and Na SEIs is the contrasting value of E_a(SEI) measured at the early stages of the SEI formation (Table 1). The measured E_a values support the claim that Na SEIs are more porous than Li SEIs, since the E_a values of solid-state SEI compounds are much higher than and the ones of the liquid electrolytes (see ESI, Tables S1 and S2‡). Furthermore, the measured effective ionic conductivities of the SEI (σ_{SEI}) calculated from the SEI geometry (Table 1) and the measured resistance in the systems are at least four orders of magnitude higher than the ionic conductivity values of Li/Na single inorganic SEI compounds (Tables S1 and S2‡). As already mentioned in our previous work, the higher porosity of the Na SEI in contrast to the Li SEI is most likely attributable to the volume effects during the passivation layer formation characterized by the Pilling–Bedworth ratios (R_{PB}, the molar volume ratio between the SEI compounds and the metal). These are smaller than unity for the relevant Na SEI compounds.[44] Naturally, the liquid electrolyte in the channel (termed channel liquid) is not expected to be thermodynamically stable against the alkali metals, giving rise to reaction layers at the metal surface. However, such layers must be thin, in particular initially, so that their resistance contribution remains negligible.

Let us start with the general morphological conception which will later serve as an adequate guide for the two cases (Li, Na) we refer to experimentally. We consider an alkali metal electrode in contact with an electrolyte, which gives rise to formation of a passivation layer (*e.g.* SEI) which – for simplicity – we assume to be chemically homogeneous. We assume that there is an opening in the SEI in which again an unprotected contact of the electrolyte to the electrode occurs and SEI forms within the opening. Let us now discuss the fate of this layer. We distinguish between two extreme scenarios, in an ideal case dictated by the molar volume change during the SEI formation reaction. In the first case, if the opening in the SEI is small, it plays a role of a film perturbation. Then, in a diffusion-

Table 1 Summary of the activation energies of ionic transport through SEI (E_a), effective SEI conductivities (σ_{SEI}), and SEI capacitances derived from the EIS measurement (C_m) in the symmetric Li/Na cells in contact with glyme- and carbonate-based liquid electrolytes stored under OCP condition for 2 hours. σ_{SEI} was calculated from $\sigma_{SEI} = \frac{d_{SEI}}{R_{SEI}A}$, where d_{SEI} is SEI thickness, R_{SEI} is the measured SEI resistance and A is the known geometric surface area of the electrode. Note that E_a, R_{SEI} and d_{SEI} values are from our previous study, ref. 44. C_m was calculated from $C_m = \frac{1}{2\pi f_{max} R_{SEI}}$, where f is the peak frequency in which the $|Z_{Im}|$ value becomes a maximum for the semicircle corresponding to R_{SEI}

System	E_a(SEI)/eV	σ_{SEI}/S cm^{-1}	C_m/F
Li|1 M LiTf in triglyme|Li	0.52	2.20×10^{-7}	8.33×10^{-7}
Li|1 M LiTf in EC/DMC|Li	0.55	1.92×10^{-7}	8.79×10^{-7}
Na|1 M NaTf in triglyme|Na	0.15	5.24×10^{-5}	5.52×10^{-6}
Na|1 M NaTf in EC/DMC|Na	0.30	4.64×10^{-7}	1.25×10^{-6}

controlled SEI growth case, where growth decreases with the layer thickness, the opening is quickly filled, and a continuous smooth layer is formed. The opposite occurs in the second case, if the molar volume change is significant. Here such an opening in the SEI occurs by necessity, namely, to accommodate the mismatch of the molar volumes. The newly formed product at the fresh contact will face the same mechanical problem leading to a formation of smaller openings in this thin internal layer. As the argument applies to even smaller dimension in this extremely simplified scenario, a self-similar structure is expected. Of course, the reality will restrict this self-similarity to a few steps only, and the growth will be additionally affected by island formation. Below we will put the model on a more realistic footing by inclusion of lateral agglomeration of initially formed islands.

Fig. 1a provides the simplified schematics of the SEI structure showing an opening (channel) in the SEI in which liquid electrolyte infiltrates into the bulk SEI. Bulk SEI represents the thick and resistive SEI. In the channels both the solid and liquid parts are present. The resistances and capacitances corresponding to these contributions are noted as $R_{\mathrm{SEI,bulk}}$, $C_{\mathrm{SEI,bulk}}$ (for bulk SEI), $R_{\mathrm{solid,channel}}$, $C_{\mathrm{solid,channel}}$ (for the solids in channel), and $R_{\mathrm{liquid,channel}}$, $C_{\mathrm{liquid,channel}}$ (for the liquid electrolyte in channel). Depending on the E_{a}(SEI) values of the investigated system (Table 1), two different cases of the equivalent circuit model are taken into account, as shown in Fig. 1b and c. The first case applies for the E_{a}(SEI) value which is comparable to the one of the liquid electrolyte, in our case for Na|1 M NaTf in triglyme|Na, where $R_{\mathrm{solid,channel}} \ll R_{\mathrm{liquid,channel}}$ is valid. Thereby, the contributions from both $R_{\mathrm{solid,channel}}$ and $C_{\mathrm{solid,channel}}$ may be neglected (see ESI, Fig. S2‡ for more details) and the equivalent circuit model is given in Fig. 1b. The second case can be applied for the E_{a}(SEI) values between E_{a}(liquid electrolyte) and the E_{a}(solid SEI compounds), where both the contribution from the solid and the liquid in the channel should be taken into account (Fig. 1c). In both cases, an apparent conductivity of the liquid in the channel ($\sigma_{\mathrm{liquid,channel}}$) can be estimated based on the measured frequency range (Fig. S1‡), and turns out to be three orders of magnitude lower than the one of bulk liquid electrolyte ($\sigma_{\mathrm{liquid,channel}} = 2\pi\varepsilon_0\varepsilon f_{\mathrm{peak}} < 1.7 \times 10^{-6}$ S cm^{-1}), where f_{peak} is a peak frequency in which the $|Z_{\mathrm{Im}}|$ value becomes a maximum and ε_0 is the vacuum permittivity. ε is the dielectric constant of liquid electrolyte, which is typically smaller than 30.[55,56] As such a low value of ionic conductivity of liquid electrolyte seems unlikely, the so far

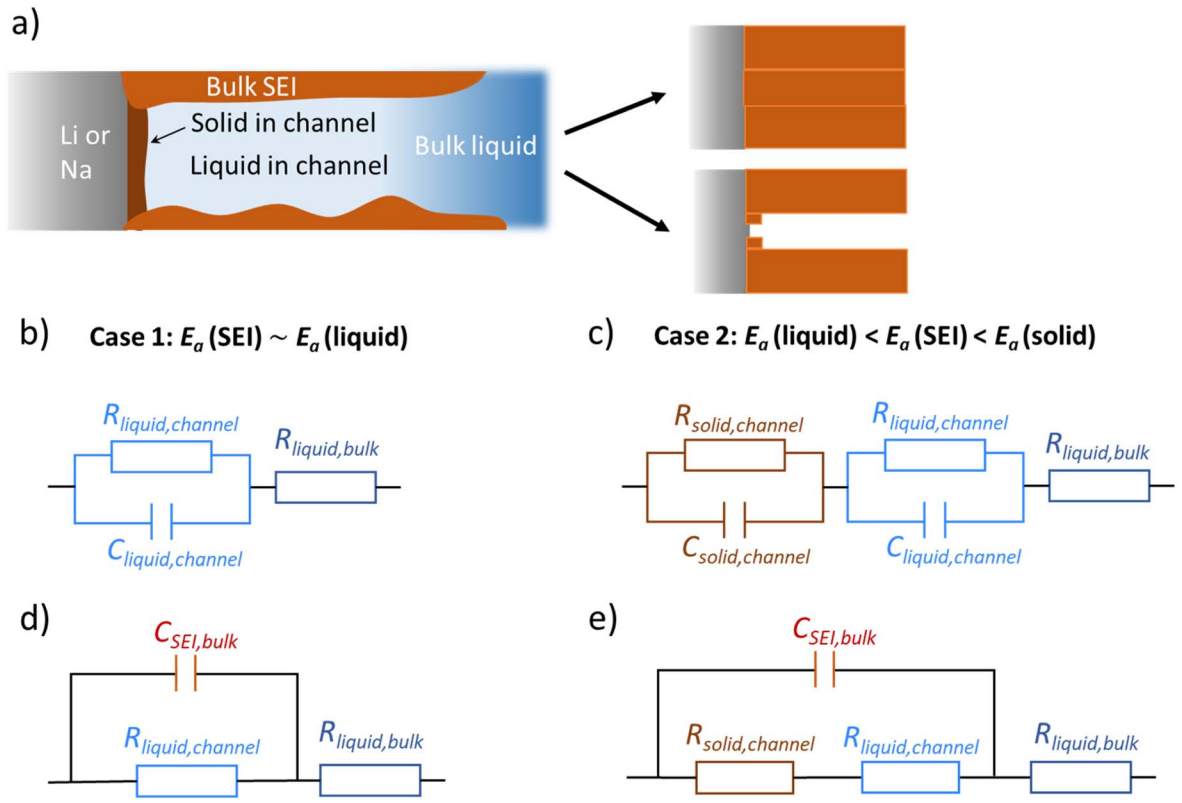

Fig. 1 (a) Faith of an opening in a passivation layer in which an interior SEI is being formed. Formation of a dense layer by quick pore filling (*e.g.* morphological stability, right up). Formation of a self-similar layer (right, down). Schematic diagram of the SEI consisting of liquid channels and thin SEI in the vicinity of the alkali metal (left). Bulk SEI represents the thick solid part of the SEI. Note that an unknown number of channels exist in the real SEI. (b and c) Equivalent circuit models of SEI in which only the liquid channel is considered (case 1), and the capacitances from the bulk SEI is also considered (case 2). (b) Corresponds to the case 1 of Na|1 M NaTf in triglyme|Na where E_{a}(SEI) is close to the one related to the transport in liquid electrolyte, (c) corresponds to the case of Li|1 M LiTf in triglyme|Li, Li|1 M LiTf in EC/DMC|Li and Na|1 M NaTf in EC/DMC|Na, where E_{a}(SEI) is in between the E_{a}(liquid) and the one related to the solid SEI compounds. (d) and (e) Represent for the situation where capacitance from the bulk SEI is taken into account, while the capacitances from the solid and the liquid present in the SEI channel are neglected.

neglected solid parallel part of the SEI should be taken into account in the equivalent circuit. Its conductance ($1/R_{SEI,bulk}$) must still be negligible, as the measured liquid-like activation energy indicates. If the resistance is considered, the discrepancy between $\sigma_{liquid,channel}$ and $\sigma_{liquid,bulk}$ would be even larger. However, the parallel capacitance ($C_{SEI,bulk}$) should matter, as the area fraction of the parallel channels is expected to be small. If the $C_{SEI,bulk}$ is taken into account, as shown in Fig. 1b and c (bottom), the conductivities of the channel-liquid and bulk-liquid become more similar. According to the measured SEI resistance values, $C_{liquid,channel}$ is estimated to be in the order of 10^{-13} to 10^{-10} F $\left(C_{liquid,channel} = \frac{\varepsilon\varepsilon_0}{R_{liquid,channel}\sigma_{liquid,channel}},\ R_{liquid,channel} < R_{SEI}\right)$. The measured capacitance values $\left(C_m = \frac{1}{2\pi f_{peak} R_{SEI}}\right)$ are listed in Table 1, which are four to six orders or magnitude higher than the $C_{liquid,channel}$ values. This implies that most of the capacitance stem from the solid bulk SEI, meaning that the relaxation time is determined by the resistance of the liquid channel and the capacitance of the solid bulk SEI ($\tau \cong R_{channel}$-$C_{SEI,bulk}$, see Fig. 1d and e). Detailed understanding of the pore geometry and distribution, which could possibly be achieved with cryo-TEM, would be the next logical step towards full characterization. This proved to be difficult until now, as the typical Ga ion beam FIB-SEM sample preparation technique available in our lab has not yielded suitable results due to reactivity of SEI, melting of the substrate (*e.g.* Li, Na) under the ion beam, and sample thickness limitations (ESI, Fig. S3‡). Indeed, these seem to be the typical problems other groups encounter when characterizing microstructure of SEIs on alkali metals, which may be circumvented by electrodeposition of metals on Cu TEM grid, or by using *in situ* cryo-TEM cells.[57–59] However, in these cases, the SEI structures imaged may defer from the ones occurring in real battery cells due to the differences in the cell pressure and electrolyte to electrode volume ratio.

In the second case, the resistance stemming from the channel ($R_{channel}$) can be described by a function of the resistance from the solid SEI in the channel ($R_{solid,channel}$) and the one from the liquid in the channel ($R_{liquid,channel}$) as follows:

$$R_{channel} = R_{solid,channel} + R_{liquid,channel}. \quad (1)$$

Since $E_a \approx -R\frac{\partial \ln \sigma}{\partial(1/T)}$ (where R is the gas constant, T is the temperature), eqn (1) can – using the identity $\partial \ln \sum y_i = \sum\left(\frac{y_i}{\sum y_i}\partial \ln y_i\right)$,[60] – be transformed into

$$E_a(channel) = \frac{R_{solid,channel}}{R_{solid,channel} + R_{liquid,channel}} E_a(solid, channel) + \frac{R_{liquid,channel}}{R_{solid,channel} + R_{liquid,channel}} E_a(liquid, channel) \quad (2)$$

where E_a(solid,channel) and E_a(liquid,channel) refer to the ionic transport through solid SEI layer and liquid in the channel, respectively. For E_a(channel) = E_a(SEI), eqn (2) can be rearranged in terms of the thickness ratio of the liquid part and the solid part in the liquid channel to yield

$$\frac{d_{liquid,channel}}{d_{solid,channel}} = \left(\frac{\sigma_{liquid,channel}}{\sigma_{solid,channel}}\right)\left(\frac{E_a(solid, channel) - E_a(SEI)}{E_a(SEI) - E_a(liquid, channel)}\right). \quad (3)$$

Upon additional assumption that the SEI resistance is solely dominated by the channel ($R_{SEI} = R_{channel}$), the thickness ratio $\left(\frac{d_{liquid,channel}}{d_{solid,channel}}\right)$ can be plotted as a function of E_a(solid,channel) and $\sigma_{solid,channel}$ (Fig. S4‡). The obtained results indicate that the thickness of the liquid channel is orders of magnitude higher than the one of solid part in the liquid channel, unless the solid is conductive enough ($\sigma_{solid,channel} > 10^{-6}$ S cm^{-1}, E_a(solid,channel) < 0.5 eV).

2.2. SEI growth under open circuit potential condition

In order to better understand the growth specific kinetics, the model needs refinement. Let us first consider Fig. 2 which shows the time evolution of SEI resistance (R_{SEI}), SEI capacitance (C_{SEI}, derived in the same way as it was done for C_m in Table 1) and relaxation times ($\tau = R_{SEI}C_{SEI}$) recorded under open-circuit conditions for approximately 600 hours for four characteristic systems in Fig. 2. Classic thin film growth laws are typically parabolic (diffusion-controlled) and linear (interfacially-controlled),[61,62] but the real situation might deviate from the models owing to the chemical and morphological complexity. Compared to the case of Li where relatively mild changes of R_{SEI} and C_{SEI} over time were observed (Fig. 2a–d), the Na system experiences striking changes of R_{SEI} and τ, while C_{SEI} varies less (Fig. 2e–h). We ascribe the distinguished behavior of Na compared to Li to the Pilling–Bedworth ratio as mentioned previously, implying that pores are continuously created, leading to continuous infiltration of the liquid and subsequent chemical reaction, whenever the liquid meets the naked alkali metal. For the SEI forming on Li where R_{PB} is greater than unity (in the case of several SEI compounds such as Li_2CO_3 (1.35), LiOH (1.26) and Li_2S (1.06)), more morphologically-uniform and denser SEI (compared to Na SEI) seems to be realized. The local chemical reaction at the metal/liquid contacts will lead to the SEI growth and thus to the increase of the E_a. Fig. 2 shows such an increase of R_{SEI} and E_a(SEI) values upon aging for all Li/Na symmetric cells under consideration, regardless of the used electrolytes.

The most interesting SEI growth behavior was observed in the Na symmetric cell with glyme-based electrolyte (Fig. 2e). The initial behavior of R_{SEI} (t < 280 hours) shows a long period of low resistance (few ohms) where the E_a tells us that the ion transport mechanism through liquid phase is dominant, followed by an abrupt increase of the SEI resistance and subsequent intermittent interruptions. For the purpose of examining the reproducibility of data, six Na–glyme cells were assembled and measured with the identical experimental method (ESI, Fig. S5‡). All cells showed similar R_{SEI} behavior over time (small R_{SEI} values until 100–200 hours and abrupt increase, followed by

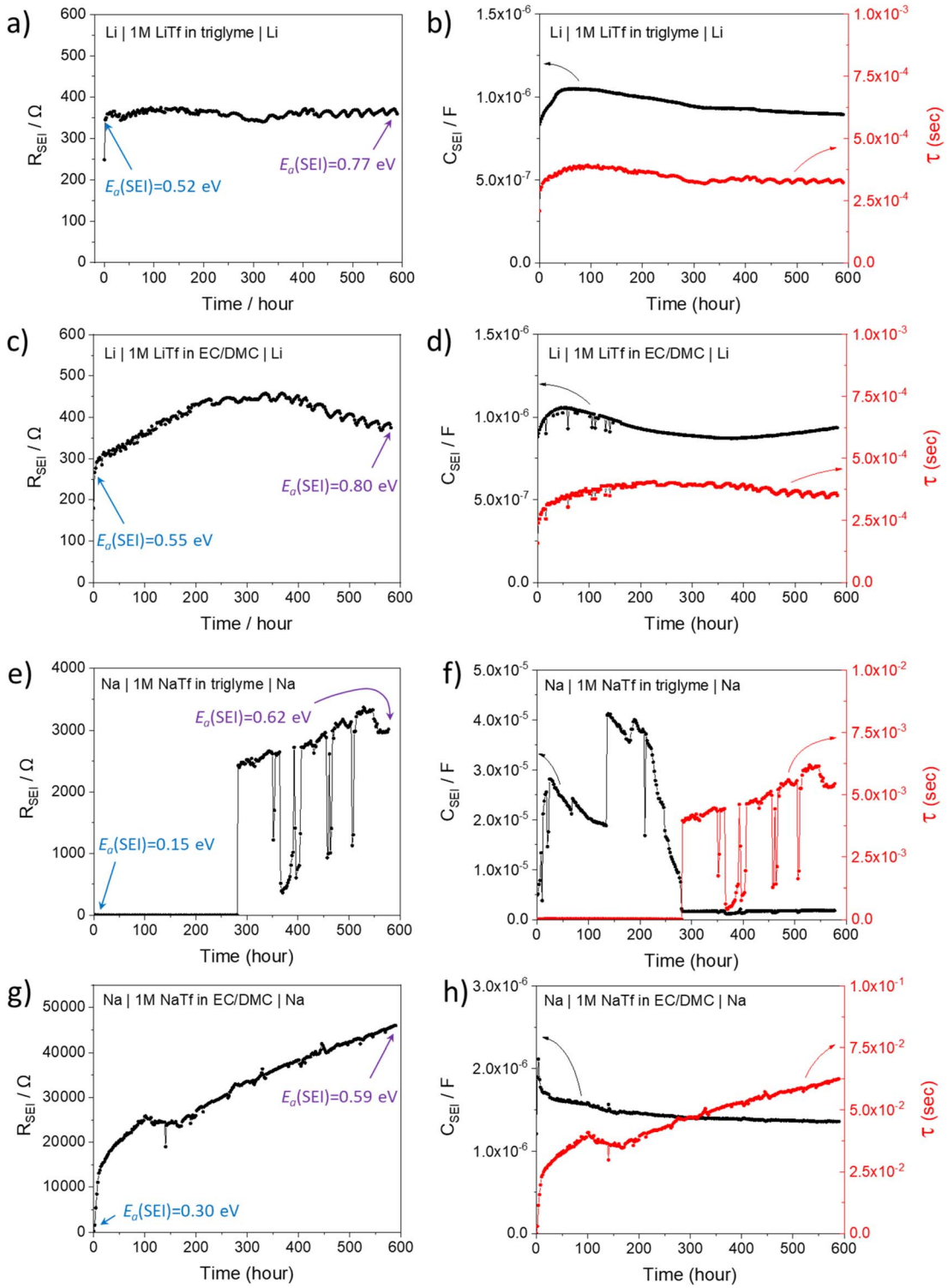

Fig. 2 Time-dependent SEI resistance (R_{SEI}), SEI capacitance (C_{SEI}) and the relaxation time ($\tau = R_{SEI}C_{SEI}$) measured in Li/Na symmetric cells with glyme-based and carbonate-based electrolytes stored under open-circuit condition. (a and b) Li|1 M LiTf in triglyme|Li, (c and d) Li|1 M LiTf|Li in EC/DMC, (e and f) Na|1 M NaTf in triglyme|Na, (g and h) Na|1 M NaTf in EC/DMC|Na. The activation energies corresponding to R_{SEI} measured by temperature-dependent EIS are denoted in (a, c, e and g). E_a(SEI) measured after 2 hours is marked as blue while the one measured after 600 hours is marked as purple.

intermittent R_{SEI} drops). The increase can be ascribed to the situation in which transport in the pore-solid becomes the rate determining step, while the abruptness may be attributable to the densification of the pores in a lateral direction, caused by the ongoing reaction in the pores or external pressure built up in the cell. The following intermittent resistance drop indicates

partial channel formation connected with the newly formed as a result of the (i) analogous mechanical instability discussed above, (ii) dissolution of the SEI,[63–65] or (iii) mechanical detachment in the course of continuous chemical reaction. If the R_{PB} values of the reaction products in the liquid channel are similar to the ones of the initial SEI formation, a continuous pore formation with a certain degree of self-similarity can be expected. This means that the sequence of infiltration, reaction, growth and cracking can be continued on a continuously smaller scale. A self-similar evolution of SEI would demand continuously lower SEI growth periods and continuously higher residual resistances, a feature that despite the over-simplification seems to be met in Fig. 3. The interpretation of the growth mechanism of SEI on Na in glyme-based electrolytes used in this study is as follows: The Na SEI is initially porous, thus the resistance is dominated by the ion transport in the liquid channel. Blocking within the liquid channels by newly formed reaction products at the Na surface connected with densification leads to the abrupt increase in resistance. The SEI-forming reaction progresses with mechanical instability of the SEI, and seemingly in a self-similar manner. Note that this picture is strongly simplified and additional kinetic pathways are possible.

Let us put this on a more quantitative level by also including lateral morphological effects. For the system under concern, we expect the formation of islands soon after contact of the electrolyte with the metal. The islands are initially isolated, but in the course of time they will form an increasingly dense layer. In this stage, this portion of a surface film can be treated as a composite of solid and liquid portions with increasing volume fraction of the solids. We then can approximate the overall resistance R_{SEI} as

$$\frac{1}{R_{SEI}} = \frac{1}{R^{\parallel}_{solid}} + \frac{1}{R^{\perp}_{solid} + \frac{g}{\varphi(\sigma_{solid}) + (1-\varphi)\sigma_{liquid}}} \quad (4a)$$

The right-hand term in the denominator of the second summand takes account of this composite contribution, with σ_{solid}, σ_{liquid} describing the conductivities of the two phases, while g is a geometrical factor standing the ratio for thickness (d) and area (A) of the composite (in the channels). $R^{\parallel}_{solid}$ is short for the resistance parallel to the channels; $1/R^{\parallel}_{solid}$ is negligible in the very beginning where the compaction affects the entire contact area, but becomes increasingly important at later stages. $R^{\perp}_{solid}$ is the series contribution of compact film portions within the channels. It can be neglected in the following. With a slight rearrangement we write

$$\frac{1}{R_{SEI,i}} = \frac{1}{R^{\parallel}_{solid,i}} + \frac{\varphi_i r + (1-\varphi_i)}{\gamma_i} \quad (4b)$$

where $\gamma \equiv g/\sigma_{liquid}$ and r is short for the ratio $\sigma_{solid}/\sigma_{liquid}$. Already this simple equation (eqn (4b)) can reproduce the complex behavior shown in Fig. 2e, if we reasonably assume that φ essentially increases linearly with time in the respective stages of compaction. The subscript i in eqn (4b) labels the respective time-stage indicated in Fig. 3. In stage 1 islands grow together all over the contact area. The very abrupt behavior observed experimentally is simply the consequence of r being very low, and it contributes only very close to $\varphi_1 = 1$.

After the abrupt R-increase (now the islands have formed a resistive, comparatively closed layer), R_{SEI} increases linearly within time (stage 2). The linearity indicates that the product formation is not determined by the flux through the product but rather by liquid transport. Note that the highly resistive film (realized in stage 2) is still not as resistive as a very dense film and exhibits an activation energy which is still lower than that of the pure solid, indicating remaining porosity. This is also seen by comparison with the resistance values of Fig. 2g. (The fact that R_{SEI} is higher than in Fig. 2a reflects the lower conductivity of the Na-compounds compared to the Li-compounds (see ESI‡)). This porous film then reaches a thickness where cracking occurs (the low mechanical strength can be attributed to the porosity). The resistance drops to a level (stage 3) that is higher than in stage 1 as the area in which now island formation occurs is much smaller, while the other parts are taken care of by $R^{\parallel}_{solid}$. Again eqn (4a) can describe the further evolution, even the curved behavior in stage 3 is well reproduced even if r remains unchanged. This is a consequence of the $(1/R^{\parallel}_{solid})$ term: initially, *i.e.*, at $\varphi_3 \simeq 0$ its influence is minimal but becomes increasingly significant with increasing time (φ_3) as the channels become more resistive. After the channel has become (partially) filled, the parallel resistance is the dominant contributor. This filling has to happen more quickly than in stage 1, as the area fraction of the channels is less than 1. If we assume $d_3 = d_1$ and σ_{solid} to remain constant, an area fraction of 10^{-4} follows for which the observed filling time appears even too long. However, one can certainly assume that the channels are not completely filled ($d_3 < d_1$) and that the final film is porous (σ_{solid} becoming higher) leading to

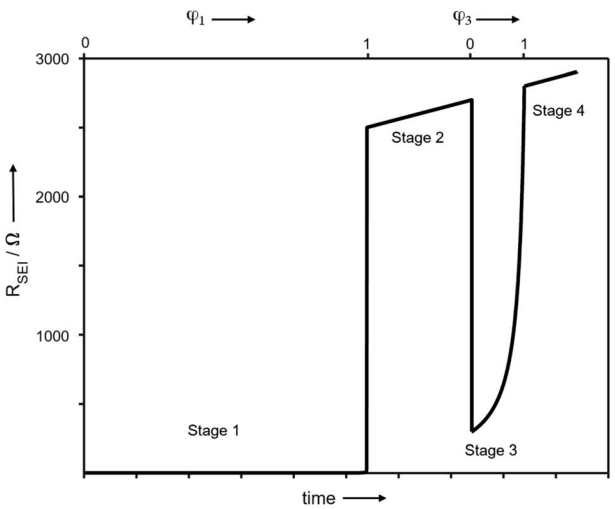

Fig. 3 Modelling of the thin film growth where volume changes are such that islands occur. Such islands grow together laterally to form a more compact film (stage 1), which then grows according to a linear growth law (stage 2). After a mechanical instability, the film cracks, and in the opening, the same scenario repeats (stage 3) *etc.* The detailed parameters are given in ESI,‡ but the comparison with Fig. 2e shows the remarkable reproduction of all the basic growth features.

a greater area fraction. The resistance of the porous SEI is nonetheless similar to that at the end of stage 2 (probably a little higher owing to the increased mass). In stage 4, linear growth dominates again, and the observed slope is similar so that the upper parts of the resistance could overall follow a linear growth law. This growth is interrupted due to mechanical instability which occurs earlier than in stage 2, owing to a higher overall inhomogeneity. As outlined before, this scenario may be expected to be continued roughly self-similarly. A more detailed analysis is given in the ESI,‡ here we just show the result for such fitting of Fig. 2e for 4 stages revealing the remarkable agreement. A more detailed description is pointless since in contrast to these characteristic patterns the details are not exactly reproduced.

The behavior in Fig. 2g is strikingly different; here approximately a square root behavior is seen, *i.e.* the film growth is rather homogeneous and determined by the flux through the film. It may be assumed that the different electrolyte chemistry renders the film mechanically tougher and probably denser due to the difference in polymeric contributions. Accordingly, the resistance is higher even though the similar activation energy may suggest still the presence of liquid-filled pores that electrically contribute. The behaviour of the capacitance (Fig. 2f) is also interesting as the absolute variations are smaller and it exhibits structures already in stage 1, before it decreases by about one order of magnitude. Such structure is expected due to the lateral phenomena discussed above. The lower values at later stages reflect the fact that parallel solid parts determine the capacitance in agreement with the equivalent circuit model (Fig. 1). The somehow opposite behavior when compared to the resistance is rooted in the opposite geometric dependence when compared to the resistance.

3. Conclusion

In this work, we treated the time-dependent impedance spectroscopy results in the light of our previous study on ion transport in SEIs concerning Li/Na storage. The striking differences between Li and Na are reflected by the E_a(SEI) values indicating the presence of large amount of liquid channels in the latter case. Based on this fact and the corresponding relaxation times of the SEI processes, we propose a very simple equivalent circuit model that takes account of channels within the SEI structure which are at least partially filled with the liquid electrolyte. As long as the solid SEI layers in the channels are highly resistive compared to the liquid in the channels, impedance is dominated by the liquid transport. Parallel contributions by the surrounding solid are then negligible in terms of the resistance, but dominate the capacitive part of the impedance. In the course of time, the reaction layers within the channels grow and the overall resistance becomes more solid-like. If the reaction layer exhibits a decreased molar volume, a self-similar growth mode may be applicable. This minimal motif of partially liquid-filled channels within a resistive but dielectrically active matrix is not only relevant for the Na cases. It can also be applied to the more coherent layers; here the motif represents perturbations that, in the course of time, get 'ironed out' (the surface flattens) because the channel solid grows faster than the surrounding (due to its thickness) until the channel is closed. Extending the model by explicitly including lateral film compaction due to agglomeration of islands can explain all the characteristic features of the complex SEI growth.

Our finding is critical especially since previous reports on Na in combination with glyme-based electrolytes suggest that the initially low values of R_{SEI} are an indication of chemo-mechanically stable and conductive SEI.[66–68] However, we show that the low values of R_{SEI} does not *per se* originate from the dense, thin and ionically conductive SEI, but in this case rather from the initially porous SEI, where the major transport pathway is the one through the liquid electrolyte in the pores, finally resulting in the SEI growth and densification. These conclusions were only possible only through detailed analysis of the impedance data. We are convinced that the experimentally based and inductively obtained description of the impedance response will help to better understand the complex issue of passivation layers in alkali metal batteries.

Data availability

The datasets supporting this article are given in previous publication (**https://pubs.acs.org/doi/full/10.1021/acsami.1c15607**) and in the ESI.‡

Conflicts of interest

There are no conflicts to declare.

Acknowledgements

The authors appreciate the help of Uwe Traub in data fitting.

References

1 H. L. F. Kawamura, M. LaFleur, K. Iversen and H. W. J. Cheng, *Frontier Technology Issues: Lithium-Ion Batteries: A Pillar for a Fossil Fuel-Free Economy?* **https://www.un.org/development/desa/dpad/publication/frontier-technology-issues-lithium-ion-batteries-a-pillar-for-a-fossil-fuel-free-economy/#:~:text=Lithium%2Dion%20batteries%20have%20indeed,or%20wind%20power%20is%20used**, 2022.

2 J. Ma, Y. Li, N. S. Grundish, J. B. Goodenough, Y. Chen, L. Guo, Z. Peng, X. Qi, F. Yang, L. Qie, C.-A. Wang, B. Huang, Z. Huang, L. Chen, D. Su, G. Wang, X. Peng, Z. Chen, J. Yang, S. He, X. Zhang, H. Yu, C. Fu, M. Jiang, W. Deng, C.-F. Sun, Q. Pan, Y. Tang, X. Li, X. Ji, F. Wan, Z. Niu, F. Lian, C. Wang, G. G. Wallace, M. Fan, Q. Meng, S. Xin, Y.-G. Guo and L.-J. Wan, *J. Phys. D: Appl. Phys.*, 2021, **54**, 183001.

3 J. Moskon, S. Drvarič Talian, R. Dominko and M. Gaberscek, *J. Electrochem. Sci. Eng.*, 2020, **10**, 79–93.

4 M. Weiss, R. Ruess, J. Kasnatscheew, Y. Levartovsky, N. R. Levy, P. Minnmann, L. Stolz, T. Waldmann, M. Wohlfahrt-Mehrens, D. Aurbach, M. Winter, Y. Ein-Eli and J. Janek, *Adv. Energy Mater.*, 2021, **11**, 2101126.

5 Y. Liu, Y. Zhu and Y. Cui, *Nat. Energy*, 2019, **4**, 540–550.
6 A. M. Colclasure, A. R. Dunlop, S. E. Trask, B. J. Polzin, A. N. Jansen and K. Smith, *J. Electrochem. Soc.*, 2019, **166**, A1412–A1424.
7 B. S. Vishnugopi, E. Kazyak, J. A. Lewis, J. Nanda, M. T. McDowell, N. P. Dasgupta and P. P. Mukherjee, *ACS Energy Lett.*, 2021, **6**, 3734–3749.
8 K. Mc Carthy, H. Gullapalli, K. M. Ryan and T. Kennedy, *J. Electrochem. Soc.*, 2021, **168**, 080517.
9 H. Nara, T. Yokoshima and T. Osaka, *Curr. Opin. Electrochem.*, 2020, **20**, 66–77.
10 M. Gaberšček, *Nat. Commun.*, 2021, **12**, 6513.
11 N. Meddings, M. Heinrich, F. Overney, J.-S. Lee, V. Ruiz, E. Napolitano, S. Seitz, G. Hinds, R. Raccichini, M. Gaberšček and J. Park, *J. Power Sources*, 2020, **480**, 228742.
12 W. Huang, D. T. Boyle, Y. Li, Y. Li, A. Pei, H. Chen and Y. Cui, *ACS Nano*, 2019, **13**, 737–744.
13 E. Barsoukov, J. H. Kim, J. H. Kim, C. O. Yoon and H. Lee, *J. Electrochem. Soc.*, 1998, **145**, 2711–2717.
14 S. Eijima, H. Sonoki, M. Matsumoto, S. Taminato, D. Mori and N. Imanishi, *J. Electrochem. Soc.*, 2019, **166**, A5421–A5429.
15 J.-F. Ding, R. Xu, C. Yan, B.-Q. Li, H. Yuan and J.-Q. Huang, *J. Energy Chem.*, 2021, **59**, 306–319.
16 A. M. Tripathi, W.-N. Su and B. J. Hwang, *Chem. Soc. Rev.*, 2018, **47**, 736–851.
17 P. Verma, P. Maire and P. Novák, *Electrochim. Acta*, 2010, **55**, 6332–6341.
18 E. Peled and S. Menkin, *J. Electrochem. Soc.*, 2017, **164**, A1703–A1719.
19 M. Nojabaee, D. Kopljar, N. Wagner and K. A. Friedrich, *Batteries Supercaps*, 2021, **4**, 909–922.
20 J. Popovic, in *Frontiers of Nanoscience*, ed. R. Raccichini and U. Ulissi, Elsevier, 2021, vol. 19, pp. 327–359.
21 X.-B. Cheng, R. Zhang, C.-Z. Zhao, F. Wei, J.-G. Zhang and Q. Zhang, *Adv. Sci.*, 2016, **3**, 1500213.
22 W. Liu, P. Liu and D. Mitlin, *Adv. Energy Mater.*, 2020, **10**, 2002297.
23 A. Wang, S. Kadam, H. Li, S. Shi and Y. Qi, *npj Comput. Mater.*, 2018, **4**, 15.
24 E. Matios, H. Wang, C. Wang and W. Li, *Ind. Eng. Chem. Res.*, 2019, **58**, 9758–9780.
25 X. Shan, Y. Zhong, L. Zhang, Y. Zhang, X. Xia, X. Wang and J. Tu, *J. Phys. Chem. C*, 2021, **125**, 19060–19080.
26 H. Wu, H. Jia, C. Wang, J.-G. Zhang and W. Xu, *Adv. Energy Mater.*, 2021, **11**, 2003092.
27 X.-B. Cheng, R. Zhang, C.-Z. Zhao and Q. Zhang, *Chem. Rev.*, 2017, **117**, 10403–10473.
28 K. J. Kim, M. Balaish, M. Wadaguchi, L. Kong and J. L. M. Rupp, *Adv. Energy Mater.*, 2021, **11**, 2002689.
29 Z. Zhang, Y. Li, R. Xu, W. Zhou, Y. Li, S. T. Oyakhire, Y. Wu, J. Xu, H. Wang, Z. Yu, D. T. Boyle, W. Huang, Y. Ye, H. Chen, J. Wan, Z. Bao, W. Chiu and Y. Cui, *Science*, 2022, **375**, 66–70.
30 M. J. Zachman, Z. Tu, S. Choudhury, L. A. Archer and L. F. Kourkoutis, *Nature*, 2018, **560**, 345–349.
31 B. Han, Z. Zhang, Y. Zou, K. Xu, G. Xu, H. Wang, H. Meng, Y. Deng, J. Li and M. Gu, *Adv. Mater.*, 2021, **33**, 2100404.
32 A. C. Thenuwara, P. P. Shetty, N. Kondekar, S. E. Sandoval, K. Cavallaro, R. May, C.-T. Yang, L. E. Marbella, Y. Qi and M. T. McDowell, *ACS Energy Lett.*, 2020, **5**, 2411–2420.
33 V. Vanpeene, J. Villanova, J.-P. Suuronen, A. King, A. Bonnin, J. Adrien, E. Maire and L. Roué, *Nano Energy*, 2020, **74**, 104848.
34 Z. Shadike, H. Lee, O. Borodin, X. Cao, X. Fan, X. Wang, R. Lin, S.-M. Bak, S. Ghose, K. Xu, C. Wang, J. Liu, J. Xiao, X.-Q. Yang and E. Hu, *Nat. Nanotechnol.*, 2021, **16**, 549–554.
35 C. Cao, M. F. Toney, T.-K. Sham, R. Harder, P. R. Shearing, X. Xiao and J. Wang, *Mater. Today*, 2020, **34**, 132–147.
36 A. J. Ilott and A. Jerschow, *J. Phys. Chem. C*, 2018, **122**, 12598–12604.
37 M. Nie, D. P. Abraham, Y. Chen, A. Bose and B. L. Lucht, *J. Phys. Chem. C*, 2013, **117**, 13403–13412.
38 A. B. Gunnarsdóttir, S. Vema, S. Menkin, L. E. Marbella and C. P. Grey, *J. Mater. Chem. A*, 2020, **8**, 14975–14992.
39 Y.-C. Hsieh, J. H. Thienenkamp, C.-J. Huang, H.-C. Tao, U. Rodehorst, B. J. Hwang, M. Winter and G. Brunklaus, *J. Phys. Chem. C*, 2021, **125**, 252–265.
40 Y. Xiang, G. Zheng, Z. Liang, Y. Jin, X. Liu, S. Chen, K. Zhou, J. Zhu, M. Lin, H. He, J. Wan, S. Yu, G. Zhong, R. Fu, Y. Li and Y. Yang, *Nat. Nanotechnol.*, 2020, **15**, 883–890.
41 F. T. Krauss, I. Pantenburg and B. Roling, *Adv. Mater. Interfaces*, 2022, **9**, 2101891.
42 R. R. Gaddam, L. Katzenmeier, X. Lamprecht and A. S. Bandarenka, *Phys. Chem. Chem. Phys.*, 2021, **23**, 12926–12944.
43 R. K. Koch, R. Kuhn, I. Zilberman and A. Jossen, *Presented in Part at the 16th European Conference on Power Electronics and Applications*, 2014.
44 K. Lim, B. Fenk, J. Popovic and J. Maier, *ACS Appl. Mater. Interfaces*, 2021, **13**, 51767–51774.
45 R. de Levie, *Electrochim. Acta*, 1963, **8**, 751–780.
46 R. de Levie, *Electrochim. Acta*, 1964, **9**, 1231–1245.
47 M. Adamič, S. D. Talian, A. R. Sinigoj, I. Humar, J. Moškon and M. Gaberšček, *J. Electrochem. Soc.*, 2018, **166**, A5045–A5053.
48 S. Drvarič Talian, J. Bobnar, A. R. Sinigoj, I. Humar and M. Gaberšček, *J. Phys. Chem. C*, 2019, **123**, 27997–28007.
49 N. Kaiser, S. Spannenberger, M. Schmitt, M. Cronau, Y. Kato and B. Roling, *J. Power Sources*, 2018, **396**, 175–181.
50 I. D. Raistrick, J. R. Macdonald and D. R. Franceschetti, in *Impedance Spectroscopy*, 2018, pp. 21–105, DOI: **10.1002/9781119381860.ch2**.
51 E. Peled, D. Golodnitsky, G. Ardel and V. Eshkenazy, *Electrochim. Acta*, 1995, **40**, 2197–2204.
52 E. Peled, D. Golodnitsky and G. Ardel, *J. Electrochem. Soc.*, 1997, **144**, L208–L210.
53 J. Thevenin, *J. Power Sources*, 1985, **14**, 45–52.
54 A. Zaban, E. Zinigrad and D. Aurbach, *J. Phys. Chem.*, 1996, **100**, 3089–3101.
55 N. Yao, X. Chen, X. Shen, R. Zhang, Z.-H. Fu, X.-X. Ma, X.-Q. Zhang, B.-Q. Li and Q. Zhang, *Angew. Chem.*, 2021, **60**, 21473–21478.

56 I. N. Daniels, Z. Wang and B. B. Laird, *J. Phys. Chem. C*, 2017, **121**, 1025–1031.
57 Y. Li, Y. Li, A. Pei, K. Yan, Y. Sun, C.-L. Wu, L.-M. Joubert, R. Chin, A. L. Koh, Y. Yu, J. Perrino, B. Butz, S. Chu and Y. Cui, *Science*, 2017, **358**, 506–510.
58 X. Wang, Y. Li and Y. S. Meng, *Joule*, 2018, **2**, 2225–2234.
59 B. Han, Y. Zou, Z. Zhang, X. Yang, X. Shi, H. Meng, H. Wang, K. Xu, Y. Deng and M. Gu, *Nat. Commun.*, 2021, **12**, 3066.
60 J. Maier and G. Schwitzgebel, *Mater. Res. Bull.*, 1982, **17**, 1061–1069.
61 K. R. Lawless, *Rep. Prog. Phys.*, 1974, **37**, 231–316.
62 M. Nojabaee, K. Küster, U. Starke, J. Popovic and J. Maier, *Small*, 2020, **16**, 2000756.
63 L. A. Ma, A. J. Naylor, L. Nyholm and R. Younesi, *Angew. Chem.*, 2021, **60**, 4855–4863.
64 M. Mandl, J. Becherer, D. Kramer, R. Mönig, T. Diemant, R. J. Behm, M. Hahn, O. Böse and M. A. Danzer, *Electrochim. Acta*, 2020, **354**, 136698.
65 R. Mogensen, D. Brandell and R. Younesi, *ACS Energy Lett.*, 2016, **1**, 1173–1178.
66 Z. W. Seh, J. Sun, Y. Sun and Y. Cui, *ACS Cent. Sci.*, 2015, **1**, 449–455.
67 L. Lutz, D. Alves Dalla Corte, M. Tang, E. Salager, M. Deschamps, A. Grimaud, L. Johnson, P. G. Bruce and J.-M. Tarascon, *Chem. Mater.*, 2017, **29**, 6066–6075.
68 M. Goktas, C. Bolli, J. Buchheim, E. J. Berg, P. Novák, F. Bonilla, T. Rojo, S. Komaba, K. Kubota and P. Adelhelm, *ACS Appl. Mater. Interfaces*, 2019, **11**, 32844–32855.